Effect of Rotation on Seeds' Self-Burial Process: Insights from DEM Simulations

Y. Tang[1]; S. Huang[2]; and J. Tao[3]

[1]Ph.D. Student, Center for Bio-Mediated and Bio-Inspired Geotechnics (CBBG), Arizona State Univ., Tempe, AZ. E-mail: ytang116@asu.edu
[2]Ph.D. Student, Center for Bio-Mediated and Bio-Inspired Geotechnics (CBBG), Arizona State Univ., Tempe, AZ. E-mail: shuang64@asu.edu
[3]Associate Professor, Center for Bio-Mediated and Bio-Inspired Geotechnics (CBBG), Arizona State Univ., Tempe, AZ. E-mail: julian.tao@asu.edu

ABSTRACT

Seeds of some flowering plants such as *Erodium* and *Pelargonium* can bury itself into the ground for future germination. The self-burial behavior is realized due to hygroscopic coiling and uncoiling of the awns. It is hypothesized that the rotating motion due to the changing of the helical structure of the awn reduces penetration resistance of the seed via breaking the local force chains in soil. In this study, this hypothesis is tested using a DEM model, which allows investigating the interaction between a penetrator and the granular material at different scales. The DEM model was first calibrated and validated using existing laboratory triaxial test data of Ottawa sand. A cone was then penetrated into the calibrated soil sample vertically with different rotational speeds. It was observed that the rotational movement can significantly reduce the penetration resistance, and the reduction becomes more pronounced at higher rotational speeds. From particle scale analysis, the force chain and particle velocity field of the soil sample were investigated, and comparisons were made among cases, which shed light on the fundamental mechanism of the reduction effect.

Keywords: bio-inspired; self-burial; rotation; penetration resistance reduction; discrete-element-method (DEM)

INTRODUCTION

Effective and efficient penetration is vital to a wide range of burrowing organisms. Different from locomotion in other media (such as air and water), it typically requires a higher level of energy to move underground. Instead of directly pushing body parts into the soil, many organisms incorporate additional features into their burrowing strategies. It has been observed that the seeds of some flowering plants (e.g., *Erodium gruinum and Pelargonium species*) can bury itself into the soil for future germination (Evangelista et al. 2011). In general, these plant seeds are produced with bristle-like appendages, called awns (see Fig.1). The seed awn has a bi-layered structure, one with active tissue, and the other with resistant tissue. The seed awn can helically coil/uncoil in response to the dry/humid environment due to the differential deformation between the inner and outer layer (Abraham and Elbaum 2013). Coiling of the seed awns free the upper portion from the surrounding soil; whereas uncoiling re-anchors the upper portion and create the thrust for the seed capsule to penetrate. By cyclically repeating the coiling/uncoiling process, the seed is buried in to the ground.

It has been reported that the seed awns of *Pelargonium* species can reduce the penetration resistance by up to 75% with a maximum rotation rate of 7 rpm and a penetrating speed of 0.2 mm/s (Jung et al.2017). A mathematical model was established to empirically correlate the granular drag of the seed awn with the relative slip velocity of the local granular particles in

quasi-static flow regime. The proposed model was validated by conical intruder penetration test into a rotating granular sample. However, the authors only focused on the quasi-static regime (slow rotational rate and penetration speed). It would be beneficial to investigate the bioinspired rotational penetration mechanism, specifically the effect of rotation upon the penetration resistance, within dynamic regime, which is close to engineering practice. On the other hand, the rotational penetration process is essentially a soil/structure interaction issue. It's beneficial to have a thorough understanding of the soil/structure interaction mechanism at multiscale so that the bioinspired rotational penetration mechanism can be translated into geotechnical terms and applications.

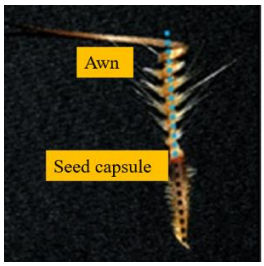

Figure 1. Seed awn of *Erodium gruinum* (modified from Abraham and Elbaum 2013)

The research described in this paper utilized the Discrete Element Method (DEM) to model the dynamic interaction between an awn-inspired rotational penetrator and the surrounding granular materials at multiscale. Parameters of the DEM model was first calibrated and validated using existing laboratory drained triaxial testing data of Ottawa sand F65. The impact of rotation rate on the penetration resistance was explored by varying rotation rate during penetration of a rod with a conical tip.

METHODOLOGY

The DEM modeling approach has been widely utilized to study the soil/structure interaction issues in engineering area (Cundall 1987). By implementing an appropriate constitute law to express the interaction between two contacting phases, the DEM model can quantitatively reproduce soil behavior and soil-structure interactions, such as the conventional cone penetration test (Jiang et al. 2014), pressuremeter test (Geng et al. 2013); and pile installation (Duan et al. 2018). It has also been used to study the soil-organism interaction problems, such as the sand-swimming behavior of the sandfish lizard (Maladen et al. 2011), and the dynamic penetration behavior of a razor-clam-inspired penetrator (Huang and Tao 2018b). Nevertheless, it is normally computational inefficient to use a DEM model to realistically simulate an engineering problem, which involves extreme levels of space and time scales and complex constitutive laws. Therefore, adopting appropriate simplifications to balance the computation effort and prediction accuracy is necessary. There are different approaches to reduce simulation times, for example, by using sphere particles, by reducing the particle modulus to increase the time step, by simplifying the constitutive laws, or by scaling up the particle sizes.

Numerical method: The open-source software YADE (Šmilauer 2015) is used for the DEM simulation tasks in this study. To enhance the computation efficiency, the granular particle is simplified as a spherical rigid ball; and a built-in linear constitutive law is implemented to describe the interaction between any two contacting particles. Basically, the movement of the particles obeys Newton's second law of motion. The Moment transfer law (MTL) (Belheine et al. 2009) is implemented to describe the surface roughness and irregularity of the sand particles.

Triaxial Test Simulation for Calibration and Validation: Based on the DEM framework implemented in YADE (Šmilauer 2015), five microscale parameters need to be calibrated: particle normal stiffness (K), stiffness ratio (α), interparticle friction angle (μ), rolling stiffness coefficient (β) and the plastic moment limit coefficient (η). The experimental results of drained triaxial compression tests on Ottawa sand F65 from (Vasko 2015) served as a reference for the calibration and validation of the five parameters.

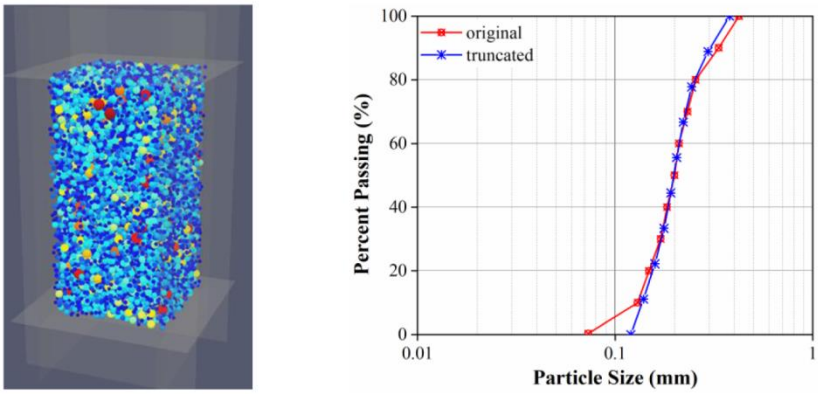

Figure 2. DEM model setup (a) triaxial test sample (b) Particle size distribution for Ottawa F65

A loose cuboid granular specimen (4mm*4mm*8mm) was generated with an initial interparticle friction angle of 41° (See Figure 2a). The particle size distribution of the specimen generally duplicates the key feature of the Ottawa sand F65 with the fine part truncated, as shown in Figure 2b. The servo control method was implemented for the application of targeted boundary confinement; and a target porosity was achieved by progressively decreasing the interparticle friction angle. Hereafter, the interparticle friction angle was reset to the desired value and the specimen was cycled to quasi-equilibrium. The numerical triaxial test was then conducted by loading the top and bottom plane towards the specimen center by maintaining a constant axial straining rate of 0.1m/s. Following the parameter calibration sequence described in (Yang et al. 2016), a set of microscale parameters that provides the best fit to the experimental results were obtained and included in Table 1.

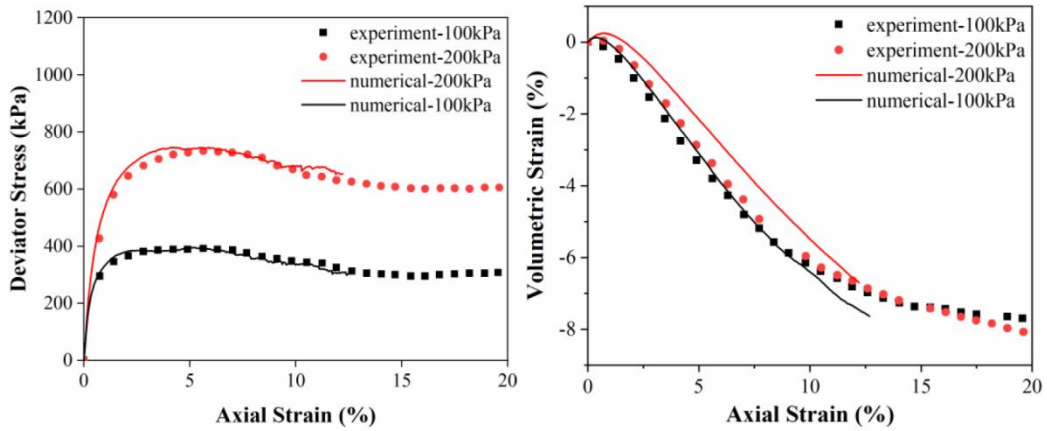

Figure 3. Triaxial compression test simulations for calibration and validation (a) deviator stress vs. axial strain (b) volumetric strain vs. axial strain

The numerical results of calibration and validation are shown in Figure 3, and compared with the experimental results (experiment-100kpa and 200kpa are used as the reference of calibration and validation, respectively). As indicated in Figure 3, using the parameters in Table 1, the numerical triaxial test results match reasonably well with the experimental results. The slight discrepancy on the volumetric strain curves in the validation set indicates that using the calibrated parameters may result in a slightly smaller dilation angle than the experimental results.

Table 1. DEM Parameters Used to Simulate the Macroscale Response of Ottawa Sand F65

Parameters	Values
Sample size (mm)	4*4*8
Number of particles in TX simulation	11526
Internal friction angle (°)	19.5
Normal stiffness (MPa)	400
Density (kg/m3)	2648
Stiffness ratio α	0.3
Confining pressure (kPa)	100,200
Porosity (ρ)	0.3682
Rolling (bending) strength (η)	0.5
Rolling stiffness coefficient (β)	0.2

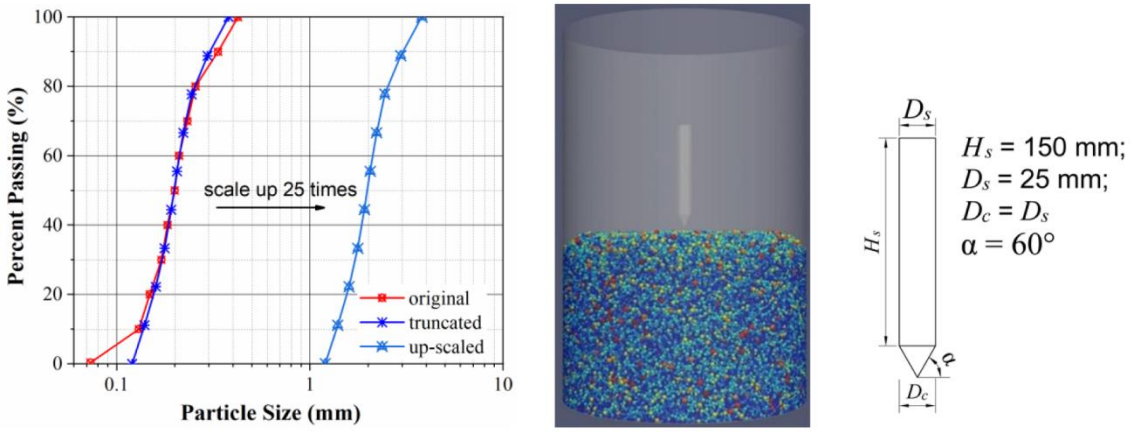

Figure 4. Simulation setup (a) Particle size distribution for penetration tests (b) penetrometer test sample (c) penetrator model

Model Construction: To construct the virtual calibration chamber, several geometric factors need to be considered (Arroyo et al. 2011): the chamber to cone diameter ratio (noted as R_d), the cone to particle diameter ratio (noted as n_p), and the sample height to the cone diameter ratio (n_h). Theoretically, using higher values of R_d, n_p and n_h will result in a larger sample size, and a higher accuracy can be achieved. However, the computational load can be dramatically increased by using a large sample for DEM simulation; also significant inhomogeneity issue appears in large DEM sample preparation and causes discrepancies in the results (Butlanska et al. 2010). A model that maintained a particle size distribution of original Ottawa F65 will result in billions of particles, which is far beyond the capabilities of our current computational resource. By using a particle size upscaling method (Butlanska 2014), it is found that there is no significant effect on the macro-scale frictional shear strength of a soil by scaling up the particle size up to 50 times in

DEM. In the penetration simulations of this study, the particle sizes were scaled up by 25 times (resulting in 46,000 particles) to reduce the computational demand (Figure 4a).

The diameter and height of the virtual calibration chamber were set as 0.4 m and 0.3m. Therefore, the R_d, n_p and n_h are 16, 5 and 5.6 respectively, which result in a low level of boundary effect but maintain a manageable computational demand and an acceptable accuracy (Figure 4b). The awn-inspired penetrator is simplified as a coaxial combination of a cylindrical shaft and a conical tip with an apex angle of 60°. The diameter of the shaft and cone were both set as 0.025 m, as illustrated in Figure 4c.

A loose granular sample was generated using a "pluviation" method within the frictionless cylindrical calibration chamber with a high initial interparticle friction angle (See Figure 4b). The targeted porosity of the generated sample was then achieved by progressively reducing the interparticle friction angle. After that, the calibrated friction angle was re-assigned to the particles, and the sample was cycled to a quasi-static equilibrium state. The awn-inspired penetrator is generated right at the top surface of the sample before penetrating into the soil. The rotational penetration kinematics is modeled as a combination of vertical penetration and rotation around the centerline of the penetrator. In this study, the vertical penetration speed for both shaft and cone was set as 0.04 m/s. Different rotation rates were considered in the simulations (40, 100, 200 and 400 rpm) in order to investigate the role of rotation on vertical penetration resistance. A control penetration case (with zero rotation rate) was conducted for the comparison purposes.

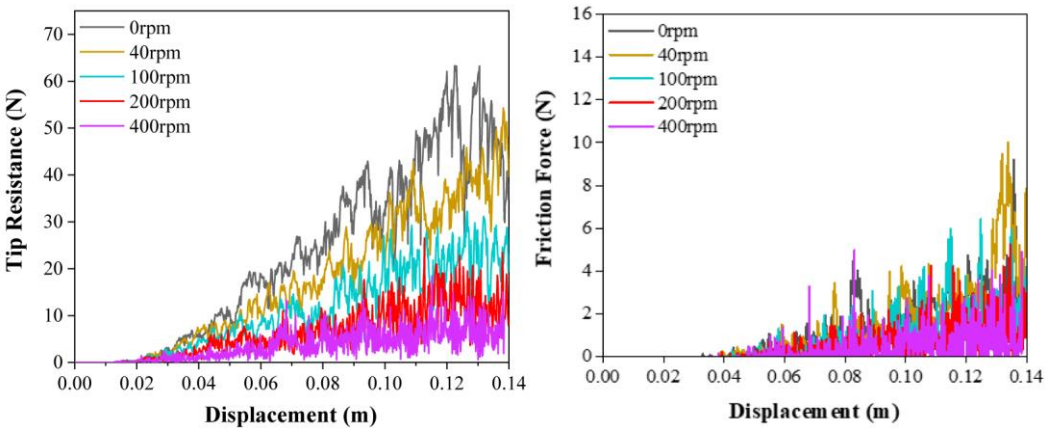

Figure 5. Resistance during penetration (a) Tip resistance applied on the cone under different rotational velocities (b) frictional force applied on the shaft under different rotational velocities

RESULTS AND DISCUSSIONS

Figure 5 presents the cone tip resistance and shaft frictional force during penetration. The data for both tip resistance and shaft frictional force are full of noisy fluctuations, which is mainly due to the low cone-particle diameter ratio and thus limited cone-particle contacts (Butlanska et al. 2010). As presented in Figure 5a, the tip resistance for all cases increases with increasing penetration depth. However, by incorporating the rotation into the penetration process, the tip resistance was reduced; and the higher the rotation rate, the smaller the tip resistance. In this study, the control case experienced the maximum tip resistance and the rotational penetration case of 400 rpm experienced the minimum. This phenomenon directly indicates that the

penetration resistance can be reduced by incorporating rotation into the penetration kinematics. It is also worth noting that the difference in tip resistance between any two neighboring cases decreases with the increasing rotation rate. In other words, the reduction of the tip resistance is not linearly correlated with the increasing rotation rate of the penetrator. Since rotation is a mechanical process and requires energy for functionality, there might be a critical rotate rate existing between 40 rpm and 200 rpm, with which the reduction of the tip resistance can be maximized with minimum energy input. Note that based on DEM simulations, (Sharif et al. 2019) also found that rotation movement can reduce the penetration resistance during the installation process of screw piles.

Force Chain Network: The contact force chain network is useful in exploring the force propagation across the entire granular system. In Figure 6, the contact force chain networks for particles lying within one cone diameter from the penetrator centerline are presented as a planar projection onto a vertical section across the chamber center axis. In order to highlight the variability of the propagated contact force corresponding to the penetrator kinematics, several measures are taken: (1) any forces lower than 0.2 N are plotted in light grey; (2) any forces higher than 6 N are colored in red; (3) the thickness of the force chains is proportional to the magnitude and representes with colors from blue to red; (4) all the force chain networks share a same color scale for an intuitive comparison among different cases.

The force chain networks are dominated by the gravitational effect initially, with concentrated strong force chains distribute along the bottom and weak force chains close to the surface; with the progress of the penetration, strong force chains appear around the advancing cone and become increasingly intensified with increasing penetration depth. The strong force chains originate from the cone surface and radiate toward the external boundary. It is interesting to find that the intensity of strong force chain around the cone for the considered rotational penetration cases becomes obviously sparser than the pure penetration case as the penetrator penetrating into a deep position (See Figure 6a, 6b, and 6c).

Similar to the tip resistance, the shaft friction resistance increases with increasing penetration depth, which is due to the increasing shaft-particle interaction area and the increasing lateral earth pressure with depth in the vertical profile (See Figure 5b). Although the large fluctuations blur the difference between different simulation cases, it can be identified that the penetration case with a rotation rate of 400 rpm experienced the minimum shaft frictional force during the penetration.

Particle Velocity Field: To further visualize the impact of rotation upon the microscale structure of surrounding granular system, the vectorized particle velocity field at the end of penetration for all the cases are illustrated in Figure 7, with the front view included in Figure 7a ~7c and bottom view included in Figure 7d~7f. Two strategies are considered to highlight the impact of rotation upon the velocity field: (1) any particles with a velocity smaller than 0.02 m/s are not included in the figure; and (2) thickness of the vectorized arrow is proportional to the magnitude of the particle velocity.

As indicated in Figure 7a, significant particle flow appears around the lower end of the shaft and cone in the pure penetration: particles around the shaft were driven by the depth-dependent interparticle friction, and particles around the cone being push downward and sideways by the advancing cone. The inclusion of rotation introduces significant particle flow around the entire rotating shaft. Meanwhile, the direction of the vectorized particle velocity is inclined laterally and downward, with an angle to the penetrator centerline (See Figure 7b). Such a phenomenon becomes increasingly augmented with the increasing rotation rate (See Figure 7c).

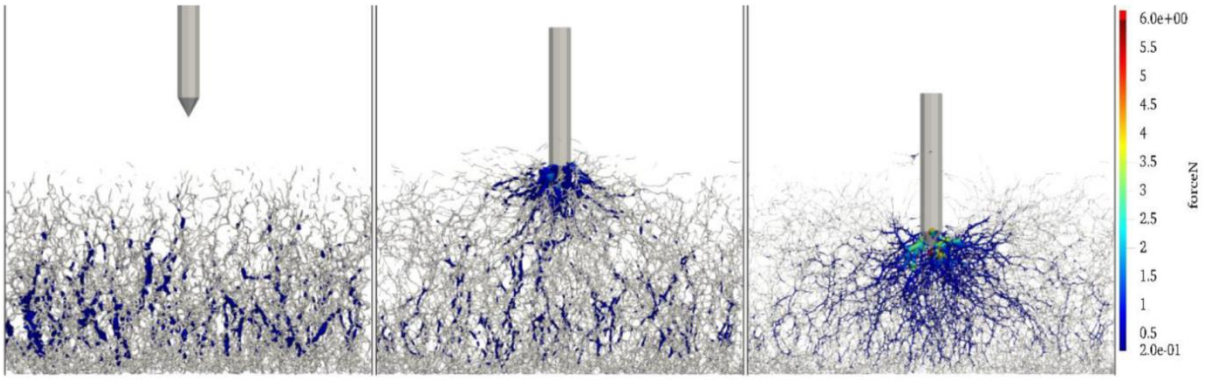

(a) force chain evolution during penetration with a rotation rate of 0 rpm

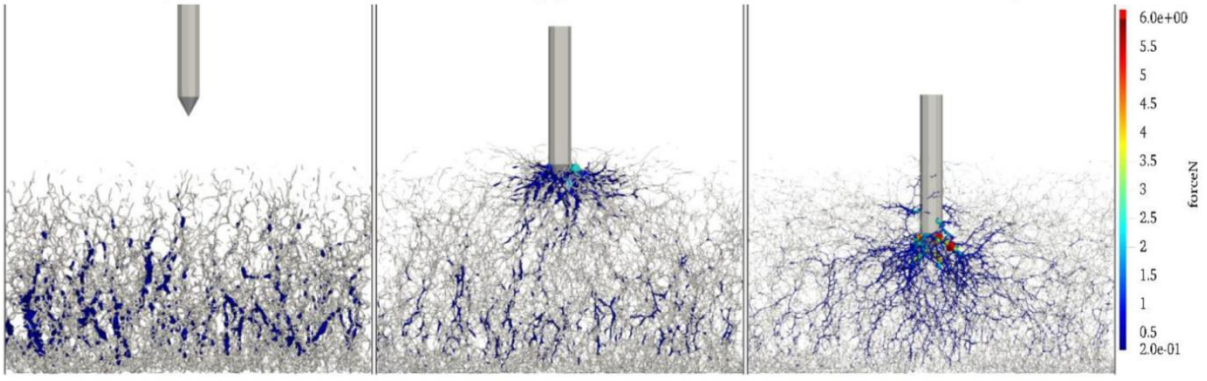

(b) force chain evolution during penetration with a rotation rate of 40 rpm

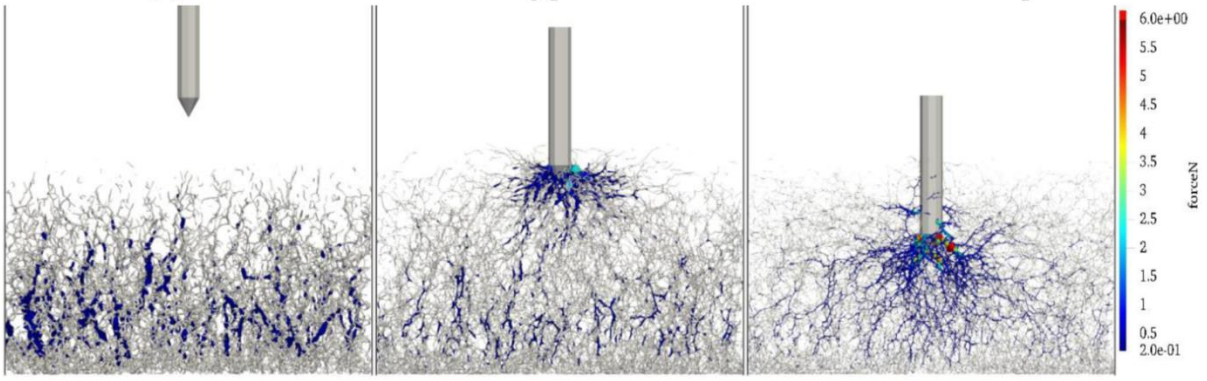

(c) force chain evolution during penetration with a rotation rate of 100 rpm

Figure 6. Force chain networks under different rotational speed

On the other hand, Figure 7d ~ 7f show the local particle flow around the cone from the bottom view. In Figure 7d, the particle flow around the cone in the pure penetration is generally in side-ways; whereas particle flow around a rotating cone tends to follow the rotating direction and become increasingly obvious when the rotating rate is getting higher (See Figure 7e ~ 7f). The rotating cone tends to shear the surrounding soil in the rotating direction, in addition to the vertical advancement induced compression and shear. This also complies with the results from Figure 5, that the tip resistance of the rotational penetration tests is smaller than the pure penetration test.

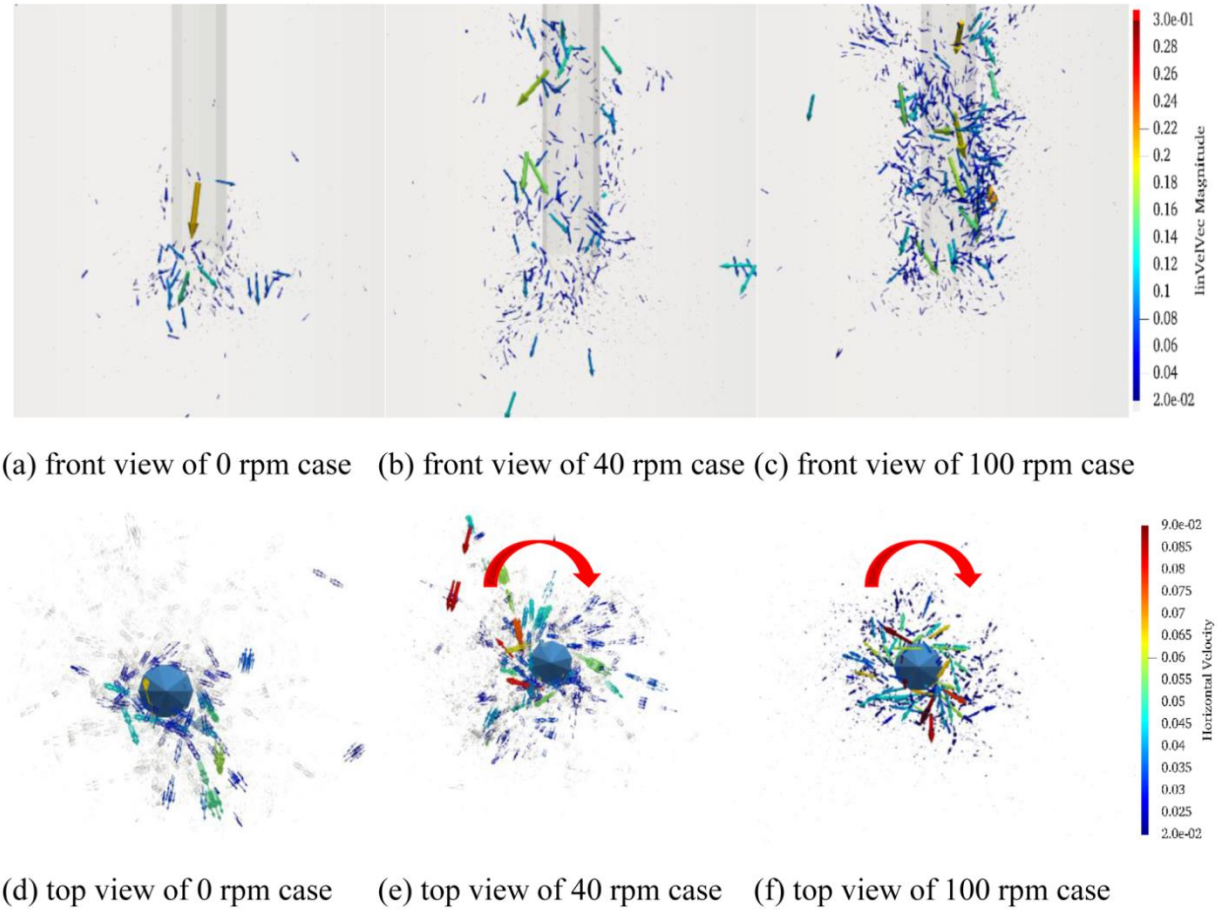

(a) front view of 0 rpm case (b) front view of 40 rpm case (c) front view of 100 rpm case

(d) top view of 0 rpm case (e) top view of 40 rpm case (f) top view of 100 rpm case

Figure 7. Particle velocity field under different penetration cases

DISCUSSION AND CONCLUSIONS

In this study, the effect of rotation on cone penetration resistance is preliminarily investigated using Discrete Element Method (DEM). The microscale parameters for the input of the DEM model were calibrated and validated using experimental results of drained triaxial compression test. The impact of the rotation upon the penetration process was assessed through the development of the cone tip resistance and shaft frictional force, the force chain evolution across the entire granular system and the local particle velocity fields around the penetrator. Results indicate that the inclusion of rotation into the penetration kinematics causes additional shearing of the surrounding soil, which is conducive to the breaking of force chain around the penetrator and result in a smaller penetration resistance. With a higher rotation rate, the tip resistance is further reduced. Since rotation also requires energy input, it is necessary to evaluate the tradeoff between energy consumption for rotation and energy saving for penetration. A critical rotating rate might exist so that the total penetration energy is minimized. In this study, the penetration process is displacement-controlled and the rotation is introduced by continuous movement of the rigid body. For seed awns, however, the rotation is due to coiling and uncoiling of a flexible body. More in-depth studies are needed to study the self-burying process itself, that is, how coiling and uncoiling actions will induce vertical movements? Existing geotechnical practices such as helical pile installation and drilling processes may provide insights on the self-burying processes of seed awns.

ACKNOWLEDGEMENT

This material is based upon work supported by the National Science Foundation (NSF) under NSF CMMI 1849674. Any opinions, findings and conclusions or recommendations expressed in this material are those of the authors and do not necessarily reflect those of the NSF.

REFERENCES

Abraham, Y., and Elbaum, R. (2013). "Hygroscopic movements in Geraniaceae: the structural variations that are responsible for coiling or bending." *New Phytologist*, 199(2), 584-594.

Arroyo, M., Butlanska, J., Gens, A., Calvetti, F., and Jamiolkowski, M. (2011). "Cone penetration tests in a virtual calibration chamber." *Geotechnique*, 61(6), 525-531.

Belheine, N., Plassiard, J.-P., Donzé, F.-V., Darve, F., and Seridi, A. (2009). "Numerical simulation of drained triaxial test using 3D discrete element modeling." *Computers and Geotechnics*, 36(1-2), 320-331.

Butlanska, J., Arroyo, M., and Gens, A. (2010). "Size effects on a virtual calibration chamber." *Numerical methods in geotechnical engineering. Edited by T. Benz and S. Nordal. CRC Press, Balkema*, 225-230.

Cundall, P. (1987). "Distinct element models of rock and soil structure." *Analytical and computational methods in engineering rock mechanics*, 129-163.

Duan, N., Cheng, Y. P., and Liu, J. W. (2018). "DEM analysis of pile installation effect: comparing a bored and a driven pile." *Granular Matter*, 20(3), 36.

Evangelista, D., Hotton, S., and Dumais, J. (2011). "The mechanics of explosive dispersal and self-burial in the seeds of the filaree, Erodium cicutarium (Geraniaceae)." *Journal of Experimental Biology*, 214(4), 521-529.

Geng, Y., Yu, H., and McDowell, G. (2013). "Discrete element modelling of cavity expansion and pressuremeter test." *Geomechanics and Geoengineering*, 8(3), 179-190.

Huang, S., and Tao, J. (2018b). "The interplay between shell opening and foot penetration of a model razor clam: Insights from DEM simulation." *B2G Atlanta 2018 Bio-mediated and Bio-inspired Geotechnics*.

Jiang, M., Dai, Y., Cui, L., Shen, Z., and Wang, X. (2014). "Investigating mechanism of inclined CPT in granular ground using DEM." *Granular Matter*, 16(5), 785-796.

Maladen, R. D., Ding, Y., Umbanhowar, P. B., Kamor, A., and Goldman, D. I. (2011). "Mechanical models of sandfish locomotion reveal principles of high performance subsurface sand-swimming." *Journal of The Royal Society Interface*, 8(62), 1332-1345.

Sharif, Y., Brown, M., Ciantia, M., Knappett, J., Davidson, C., Cerfontaine, B., ROBINSON, S., and BALL, J. (2019). "Numerically modelling the installation and loading of screw piles using DEM." *ISSPEA 2019*, 101.

Šmilauer, V., Emanuele Catalano,Bruno Chareyre,Jérôme Duriez (2015). "Yade Documentation 2nd ed. The Yade Project."

International Meeting, American Society of Agricultural and Biological Engineers, 1.

Vasko, A. (2015). *An investigation into the behavior of Ottawa sand through monotonic and cyclic shear tests*, The George Washington University.

Yang, P., O'Donnell, S., Hamdan, N., Kavazanjian, E., and Neithalath, N. (2016). "3D DEM simulations of drained triaxial compression of sand strengthened using microbially induced carbonate precipitation." *International Journal of Geomechanics*, 17(6), 04016143.